Identificationfor Buried Objects by Ground Penetrating Radar Using the Continuous Wavelet Transform

TinDuong Quoc Chanh[1, 2], DauDuong Hieu[2], Van Nguyen Thanh[1],Thuan Nguyen Van[1]

[1]*University of Science, VNU Ho Chi Minh City, Vietnam*
[2]*Can Tho University, Can Tho City, Vietnam*
Corresponding Author: Tin Duong Quoc Chanh

ABSTRACT:*In a quantitative Ground Penetrating Radar (GPR) data processing, it is necessary to determine three principal parameters: depth, position, and size of the buried objects. However, this process takes too much time because of the complex calculus stages such as: data formation, topographic correction, data filtering, amplification and some others. In addition, the determination of those parameters for buried objects using traditional GPR methods has many difficulties since this estimation depends directly on electromagnetic wave velocity in the material, and this velocity varies very complex in all directions. Especially, for close buried objects, they always superimpose upon each other not only in the spatial domain but also in the frequency domain, making the identification for these objects significantly problematic. In this paper, the wavelet transform modulus maxima (WTMM) with the selective wavelet functions are introduced to process the GPR data, thereby it is easy to estimate the depth, size and position of the buried objects without the consideration of the electromagnetic wave velocity in the material. This GPR analysis can be applied for designing and mapping urban underground construction works.*
KEYWORDS: *GPR data processing,close buried objects, electromagnetic wave velocity, selective wavelet functions, urban underground construction works.*

I.   INTRODUCTION

In recent years, GPR has been a kind of rapid developed equipment which is useful tool to detect underground targets with many advantages, for example, non-destructive, fast data collection, high precision and resolution. It is widely used in shallow structure research such as: forecast landslide, subsidence, mapping urban underground works, traffic design, construction, archaeology and other various fields of environment. Therefore, the method for GPR processing has been developed increasingly.

Wavelet transforms originated in geophysics in the early 1980s for the analysis of seismic signals (Kumar *et al*, 1997). Since then, considerable mathematical advances in wavelet theory have enabled a suite of applications in numerous fields. In geophysics, wavelet has becoming a very useful tool because it demonstrated its outstanding capabilities in interpreting nonstationary processes that contains multiscale features, detection of singularities, explanation of transient phenomena, fractal and multifractal processes, signal compression, and some others (Kumar *et al*, 1997; Ouadfeul, 2006; Ouadfeul, 2007; Ouadfeul*et al*, 2010). It is anticipated that in the near future, significant further advances in understanding and modeling geophysical processes will result from the use of wavelet analyzing (Kumar *et al*, 1997). A sizable area of geophysics has been inherited the achievements of wavelet analysis that is interpretation of potential fields data. In this section, it was applied indenoising, separating of local or regional anomalies from the measurement field, determining the location of homogeneous sources and their properties (Fedi*et al*, 1998, Dau, 2013).

Recently, Sheng and his colleagues (2010) used the discrete wavelet transform to filter and enhance the GPR raw data in order to obtain higher quality profile. But these interpretative results still have a problem on velocity. By clear and careful analysis, we recognize that the GPR data structure is quite similar to potential field data structure not only form but also nature.Consequently, a new technique to process GPR data using Continuous Wavelet Transform (CWT) is applied to interpret quantitatively GPR data. GPR data is denoised by

the Line Weight Function (Fiorentine and Mazzantini, 1966), and then combine with the WTMM method (Mallat and Hwang, 1992) to find out the depth, size and position of the buried pipe, without using the speed of the electromagnetic wave in the survey environment. Especially, the proposed method has been used to distinguish adjacent buried objects not only by theoretical model but also actual data.

The second section of this paper shows theoretical background. The third section indicates the results and discussions, and finally the conclusion is discussed in the fourth section.

II. THEORETICAL BACKGROUND

2.1. Ground Penetrating Radar

Using radar reflections to detect subsurface objects in the first time was proposed by Cook, in 1960. Subsequently, Cook and other researchers (Moffatt and Puskar, 1976) continued to develop radar systems to discover reflections beneath the ground surface. The fundamental theory of ground penetrating radar was described in detail by Benson (1995). In short, GPR system sends out pulses of electromagnetic wave into the ground, typically in the 10-2000 MHz frequency range, travels away from the source with the velocity depends on material structure of the environment. When the radar wave moves, if it meets anomaly objects or layers with different electromagnetic characteristics, a part of the wave energy will reflect or scatter back to the ground. The remaining energy continues to pass into the ground to be further reflected, until it finally spreads or dissipates with depth. The reflective wave is detected by receiver antenna and saved into memory of the device to analyze and process. The traces along a transect profile are stacked vertically; they can be viewed as two-dimensional vertical reflection profiles of the subsurface stratigraphy or other buried features. When the object is in front of the antenna, it takes more time for the radar waves to bounce back to the antenna. As the antenna passes over the object, the reflection time becomes shorter, and then longer again as it goes past the object. This effect causes the image to take the shape of a curve, called a ''hyperbola''. This hyperbola is actually the image of a smaller object (like a pipe) located at the center of the curve (figure 1a, 2a, 4a, 7a).

The speed of an electromagnetic wave (v) in a material is given by (Sheng, *et al*, 2010):

$$v = \frac{c}{\sqrt{\left(\dfrac{\varepsilon_r \mu_r}{2}\right)\left(\left(1 + P^2\right)^{\frac{1}{2}} + 1\right)}} \tag{1}$$

where P shows the loss factor, it leans on the frequency of the electromagnetic wave, and is a function of conductivity and permittivity of the medium, $c = 0.2998$ m/ns is the speed of light in the vacuum, ε_r indicates the relative dielectric constant, μ_r illustrates the relative magnetic permeability ($\mu_r = 1.0$ for non-magnectic materials).

The depth of penetration (h) can be defined by correlating the velocity of the medium and the travelling time of the GPR signals. This allows the use of the following equation (Sheng, *et al*, 2010):

$$h = \frac{\sqrt{(t.v)^2 - S^2}}{2} \tag{2}$$

Where, S is the fixed distance between the transmitting and receiving antennas of the GPR system.

2.2. The continuous wavelet transform and Farshad – Sailhac wavelet function

The continuous wavelet transform(CWT) of 1-D signal $f(x) \in L^2(R)$ can be given by:

$$W(a,b) = \frac{1}{\sqrt{a}} \int_{-\infty}^{+\infty} f(x)\overline{\psi}\left(\frac{b-x}{a}\right)dx = \frac{1}{\sqrt{a}}\left(f * \overline{\psi}\right) \tag{3}$$

Where, $a, b \in R^+$ are scaleand translation (shift)parameters, respectively; $L^2(R)$ is the Hilbert space of1-Dwave functions havingfinite energy; $\overline{\psi}(x)$ is the complex conjugate function of $\psi(x)$,an analyzing functioninside the integral (3), $f * \overline{\psi}$ expresses convolution integral of $f(x)$ and $\overline{\psi}(x)$. In particularly, CWT can operate with various complex wavelet functions, if the wavelet function curve looks like the same form of the original signal.

To determine the boundary from anomaly objects, and then estimate their depth, size and position, thecomplex wavelet function called Farshad - Sailhac (Tin and Dau, 2016) was used. It is given by:

$$\psi^{(FS)}(x) = \psi^{(F)}(x) + i\,\psi^{(S)}(x) \tag{4}$$

Where, $\psi^{(F)}(x) = \dfrac{4 - 2x^2}{\left(x^2 + 2^2\right)^{\frac{5}{2}}} - \dfrac{1 - 2x^2}{\left(x^2 + 1^2\right)^{\frac{5}{2}}} \tag{5}$

$$\psi^{(S)}(x) = Hilbert(\psi^{(F)}(x)) \qquad (6)$$

2.3. The wavelet transform modulus maxima (WTMM) method

In image processing, determination of the edge is a considerable task. According to image processing theory, the edges of image are areas with rapid change sharply of light intensity or color contrast. For the space signal, like GPR data, the points where the amplitude of the signal quickly or suddenly changed are considered to the boundaries. Edge detection technique depended on the CWT was proposed by Mallat and Hwang (1992) correlated to construct of the module contours in the CWT coefficients on the signals to be analysed. To apply this technique, the implemented wavelet functions should be produced from the first or second derivative of a feature function which related to transfer field in the of potential field problems. Farshad - Sailhac wavelet function was proven to satisfy the requirements of the Mallat and Hwang method, so the calculation, analysis and interpretation forGPR data arecounted on the module and phase component of the wavelet transform. The edge detection technique bases on the locations of the maximum points of the CWT coefficients in the scalogram. Accordingly, the edge detection technique using CWT is also called the "wavelet transform modulus maxima" method. Analyze GPR data using WTMM is the modern technique for the detection of depth, size and position of the buried objects.

2.4. Line Weight Function (LWF)

LWFis the linear combination between Gaussian function and the second spatial derivative of Gaussian function (Fiorentine and Mazzantini, 1966):

$$l(\frac{x}{\sigma}) = C_0 h_0(\frac{x}{\sigma}) + C_2 h_2(\frac{x}{\sigma}) \qquad (7)$$

Where, Gaussian function $h_0(\frac{x}{\sigma})$ has a form: $\quad h_0(\frac{x}{\sigma}) = \frac{1}{\sigma\sqrt{\pi}}\exp\left(-\frac{x^2}{2\sigma^2}\right) \qquad (8)$

And $h_2(\frac{x}{\sigma})$ indicates the second spatial derivative of Gaussian function:

$$h_2(\frac{x}{\sigma}) = \frac{1}{\sqrt{8\pi\sigma^2}}\left(-\exp\left[-\frac{x^2}{2\sigma^2}\right] + \frac{x^2}{\sigma^2}\exp\left[-\frac{x^2}{2\sigma^2}\right]\right) \qquad (9)$$

The LWF has beenapplied effectively to denoise and enhance the contrast in the edges detection method using CWT technique (Dau, 2013).

2.5. The process for GPR data analysis using the wavelet transform

The determination of the horizontal position, the depth and the size of the buried object using Farshard - Sailhac wavelet transform can be summarized in the process including the following steps:

Step 1: Selecting an optimal GPR data slice to analyze.

After processing the raw data, we are going to obtain a GPR section quite clear and complete. The sectional data is a matrix $[m \times n]$ including m rows (corresponding to the number of samples per trace) and n columns (corresponding to the number of traces). The number of traces relies on the length of data collection route and the trace spacing (dx). The number of samples per trace is decided by the depth of the survey area and the sampling interval (dt). From the GPR section, an optimal data cutting layer is chosen (matching with a row in the matrix)to analyze by the wavelet method. Choosing this data cutting layer depend on the analyzing experience, by testing with many different layers by theoretical models as well as experimental models. The edges of buried objects will be determined exactly, if an appropriate data slice is selected.

Step 2: Denoising data by the LWF.

The appropriate data is denoised by the LWF for resolution increasing in WTMM method.

Step 3: Removing unwanted data after filtering.

The new data set after the filtering contains interpolated data near the boundary, and that is unwanted data due to the boundary effect. Therefore, it should be removed to gain an adequate data.

Step 4: Performing Farshad - Sailhac wavelet transform of GPR denoised signals by LWF.

After complex CWT, there are four distinct data sets: real part, virtual component, module factor, and phase ingredient. Module and phase data will be used in the next step.

Step 5: Changing the different scales (a) and repeating the multiscale CWT.

Step 6: Plotting the module and phase contours of the CWT coefficients with different scales (a).

The steps from 1 to 6 are operated by the modules program and run by Matlab software.

Step 7: Determining the depth, size and location of the buried pipe.

On the plot of wavelet module contours, the maximum point of the wavelet transform coefficients will be found. The horizontal and vertical coordinate of this point will be *B* and *A* respectively. The location and depth of the buried pipe will be detected by following equations:

$x = B \times dx$ (10)

$z = A \times dx$ (11)

Similarly, left and right edge coordination of the buried object will be found on the plot of wavelet phase contours and the size of the buried pipe will be estimated by:

$D = (right\ edge\ coordinate - left\ edge\ coordinate) \times dx$ (12)

III. RESULTS AND DISCUSSIONS

3.1. Theoretical models

To verify the reliability of the proposed method, many different theoretical models have been tested on including: the anomaly objects are pipe as well as square in shape made from various materials such as plastic, metal and concrete… These objects are also designed in numerous dissimilar sizes and their structures are very close to the actual models buried in the distinct environment (from homogeneous to heterogeneous). Moreover, closeburied objects in the survey environment also have been tested. The relative errors of dimension estimation from these models are acceptable from the calculus limits showing that the proposal method is reliable. However, in this paper, two models are introduced for typical treatment results.

3.1.1. Model 1 – Plastic pipe in heterogeneous environment

In this model, using antenna frequency 700 MHz, heterogeneous environment including three layers. The first layer, asphalt has thickness 0.15 m, conductivity$\sigma = 0.001$ mS/m, relative permittivity $\varepsilon_r = 4.0$, relative permeability $\mu_r = 1.0$, electromagnetic wave velocity$v_1 = 0.15$ m/ns(Van and Giang, 2013). The second layer,breakstone has thickness 0.25 m, $\sigma = 1.0$ mS/m, $\varepsilon_r = 10.0$, $\mu_r = 1.0$, $v_2 = 0.10$ m/ns. The final layer, clay soil has thickness 4.60 m, $\sigma = 200$ mS/m, $\varepsilon_r = 16.0$, $\mu_r = 1.0$, $v_3= 0.07$ m/ns. Underneath anomaly object is the plastic pipe: $\sigma = 1.0$mS/m, $\varepsilon_r= 3.0$, $\mu_r = 1.0$, $v' = 0.17$ m/ns, inside contains the air, the center of the object is located at horizontal coordination $x = 5.0$ m and vertical coordination $z = 0.55$ m, inside pipe diameter $d = 0.18$ m, outside pipe diameter $D = 0.20$ m.The measurement on the ground goes through the pipe and the length of the profile is 10.0m, with the step size of $dx = 0.03788$ m.

Figure 1a is a graph of electromagnetic waves pulse from the model 1. This graph indicates the GPR profile selected by the 700 MHz frequency antenna. According to the information is provided by the graph, a hyperbolic peak is found at (t = 9.3 ns, x = 5.0 m). Itillustrates that the reflected signal from the plastic pipe which is buried in the heterogeneous environment.

From the electromagnetic wave pulse diagram in the Fig. 1a, an optimal data slice beneath the hyperbolic peak is selected (corresponding the position of the anomaly object). The obtained result in Fig. 1b shows the signal of a selected slice.
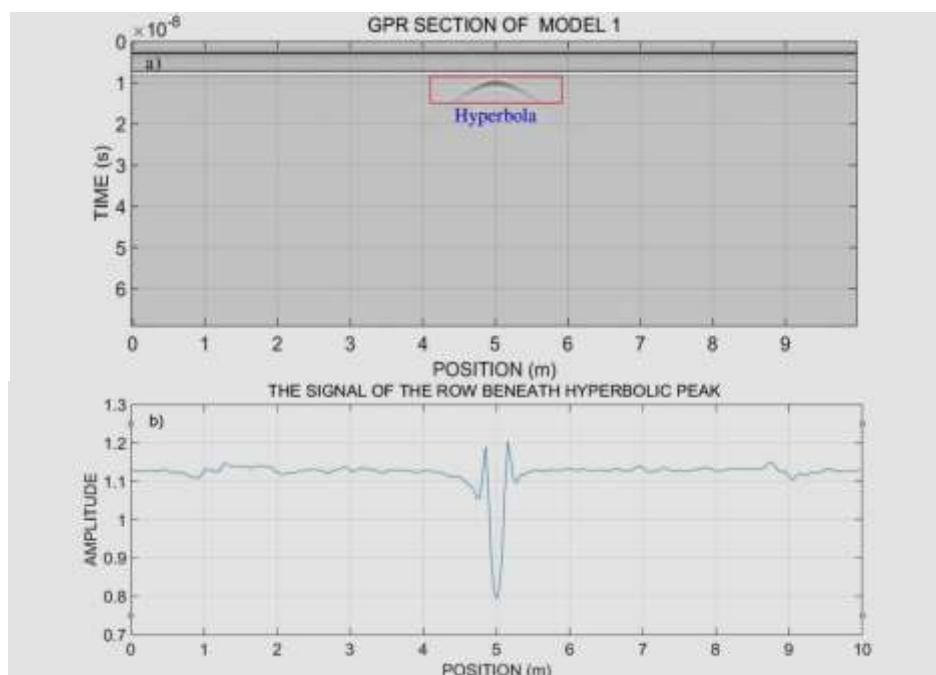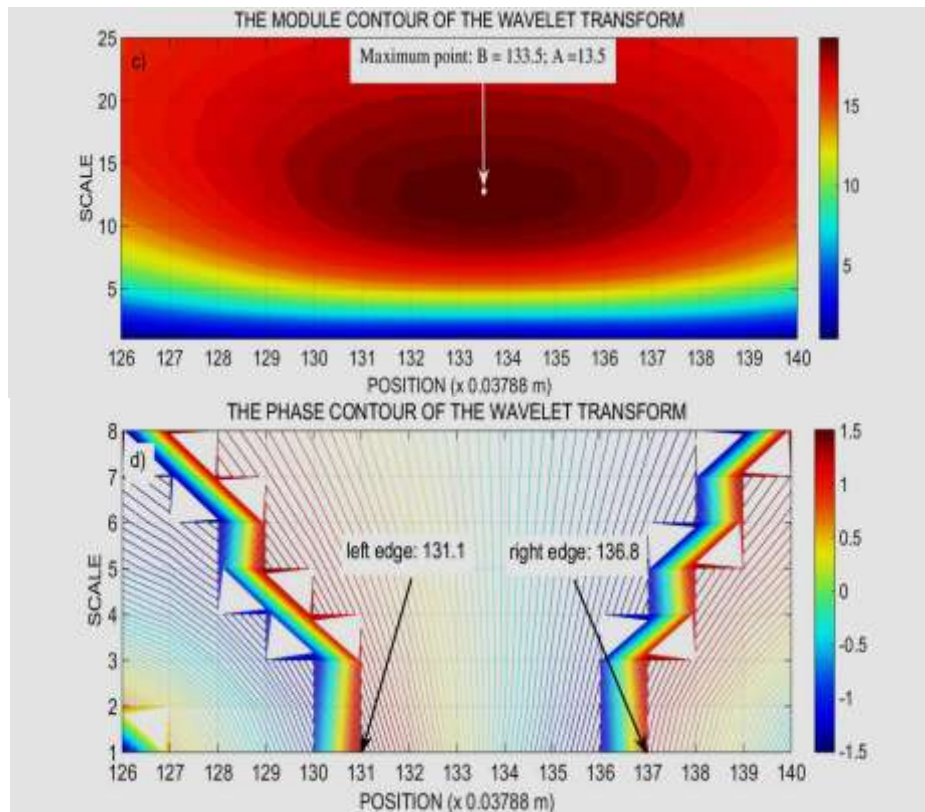
Fig. 1. The graphs of the model 1. a) GPR section of the model 1; b) The signal of the row beneath hyperbolic peak; c) The module contour of the wavelet transform; d) The phase contour of the wavelet transform.

After performing a continuous complex wavelet transform, four different sets of data are obtained, in which the data components of the module and phase are used to plot the module contour and phase contour. The results of module contour and phase contour are described in Fig. 1candFig.1d in turn.

As can be seen in the figure 1c, the center of the anomaly object is easily found at ($B = 133.5$; $A = 13.5$). In addition, the left edge and the right edge coordination of the anomaly object are presented at 131.1, 136.8 respectively in the figure 1d.

Therefore, the position, depth and size of the pipe are determined by the equation (10), (11) and (12). Thecalculativeresultsare representedin table 1.

Table 1: Interpretative results of the model 1

Position	x= $133.5 \times 0.03788 = 5.057$ m	Relative error	1.1%
Depth	z = $13.5 \times 0.03788 = 0.511$ m	Relative error	7.1%
Size	D = $(136.8-131.1) \times 0.03788 = 0.216$ m	Relative error	8.0%

3.1.2. Model 2 – Metal pipe and concrete cylinder in homogeneous environment

In this model, using antenna frequency 250 MHz, unified environment, dry sand has thickness 5.0 m, $\sigma = 0.01$ mS/m, $\varepsilon_r = 5.0$, $\mu_r = 1.0$, $v = 0.13$ m/ns. Underneath there are two adjacent objects with different parameters. Anomaly object 1 is the metal pipe : $\sigma = 100$ S/m, $\varepsilon_r = 81.0$, $\mu_r = 1.0$, $v_1 = 0.0082$ m/ns, inside contains the air, the center of the object is located at horizontal coordination $x_1 = 3.0$ m and vertical coordination $z_1 = 1.00$ m, inside pipe diameter $d_1 = 0.28$ m, outside pipe diameter $D_1 = 0.32$ m. Contrastingly, anomaly object 2 is the concrete cylinder: $\sigma = 1.0$mS/m, $\varepsilon_r = 6.0$, $\mu_r = 1.0$, $v_1 = 0.12$ m/ns, inside contains the air, the center of the object is located at horizontal coordination $x_2 = 7.0$ m and vertical coordination $z_2 = 1.20$ m, inside cylinder diameter $d_2 = 0.40$ m, outside cylinder diameter $D_2 = 0.46$ m.The measurement on the ground goes through two objects and the length of the profile is 9.0m, with the step size of $dx = 0.04298$ m.
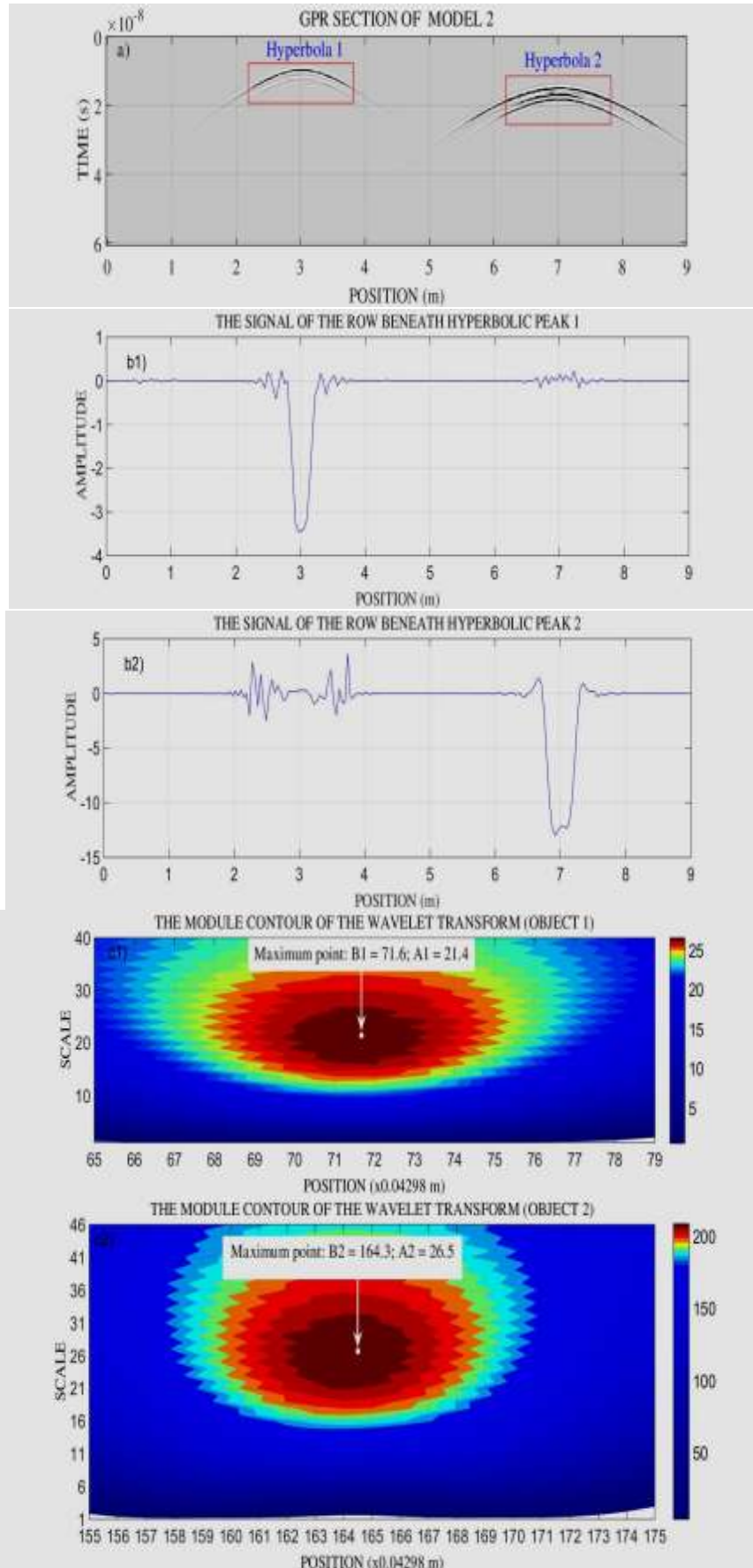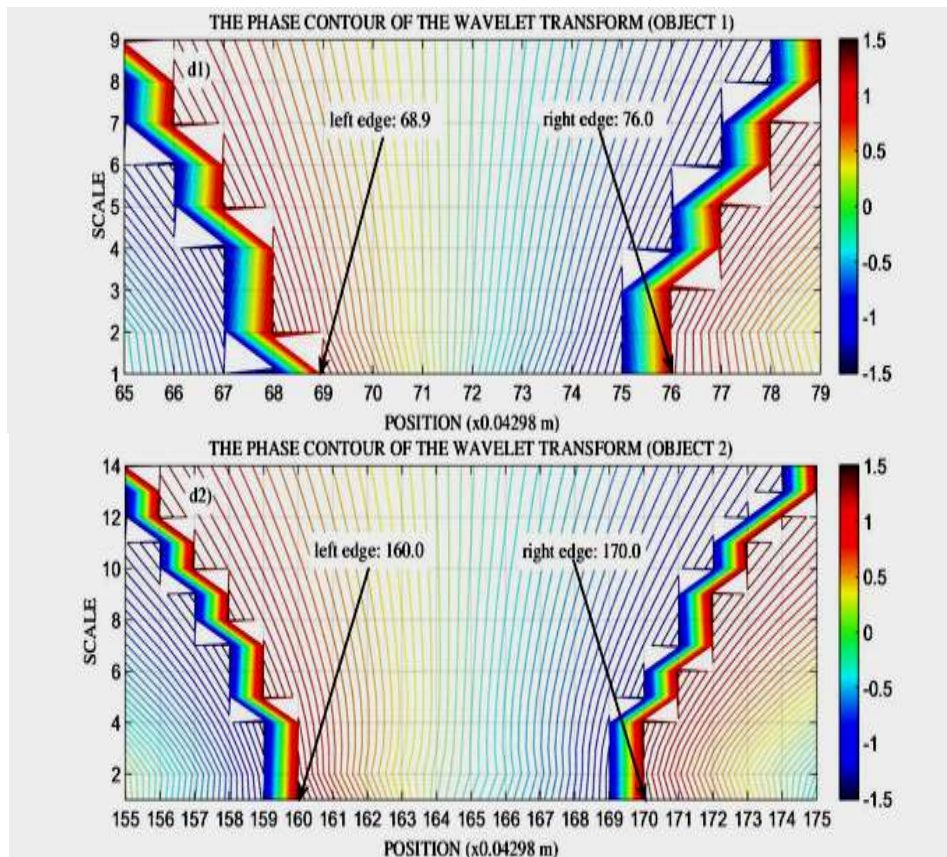
Fig. 2. The graphs of the model 2. a) GPR section of the model 2; b1 and b2) The signal of the row beneath hyperbolic peak 1 and 2; c1 and c2) The module contour of the wavelet transform corresponding object 1 and object 2; d1 and d2) The phase contour of the wavelet transform for object 1 and object 2 in turn.

Figure 2a is a graph of electromagnetic waves pulse from theoretical model. This graph shows the GPR profile selected by the 250 MHz frequency antenna. Based on the graph, two hyperbolic peaks are found at ($t_1 =$ 9.4 ns, $x_1 = 3.0$ m) and ($t_2 = 14.6$ ns, $x_2 = 7.0$ m). They indicate that the reflected signal from the metal pipe and concrete cylinder which are buried in the uniform environment. However, hyperbola 1 is more translucent than hyperbola 2 because the transmission velocity in the metal is lower than the propagation velocity in the medium and due to the influence of the strong reflected signal from the concrete cylinder.

From the electromagnetic wave pulse diagram in the Fig. 2a, the two optimal data slices beneath the hyperbolic peak 1 and hyperbolic peak 2 are selected (corresponding the position of the two anomaly objects). The obtained results in Fig. 2b1 and Fig. 2b2 illustrate the signals of the two selected slices respectively.

After performing a continuous complex wavelet transform, four different sets of data are obtained, in which the data components of the module and phase are used to plot the module contour and phase contour. The results of module contour and phase contour are described in Fig. 2c1, Fig. 2c2 and Fig. 2d1, Fig. 2d2 in turn.

According to the results plotting of the module in the figure 2c1, the center of the anomaly object 1 is easily found at ($B_1 = 71.6$; $A_1 = 21.4$). Furthermore, the left edge and the right edge coordination of the anomaly object 1 are presented at 68.9, 76.0 respectively in the figure 2d1. Similarly, the center of the anomaly object 2 is also found at ($B_2 = 164.3$; $A_2 = 26.5$) in the Fig. 2c1. In addition, the left edge and the right edge coordination of the anomaly object 2 are located at 160.0, 170.0 respectively in the Fig. 2d2.

So, the position, depth and size of the pipes are determined by the equation (10), (11) and (12). Thecalculativeresultsare representedin table 2.

Table 2: Interpretative results of the model 2

Position	$x_1 = 71.6 \times 0.04298 = 3.077$ m	Relative error	2.6%
	$x_2 = 164.3 \times 0.04298 = 7.062$ m	Relative error	0.9%
Depth	$z_1 = 21.4 \times 0.04298 = 0.920$ m	Relative error	8.0%
	$z_2 = 26.5 \times 0.04298 = 1.139$ m	Relative error	5.1%
Size	$D_1 = (76.0\text{-}68.9) \times 0.04298 = 0.305$ m	Relative error	4.7%
	$D_2 = (170.0\text{-}160.0) \times 0.04298 = 0.430$ m	Relative error	6.5%

The calculative results in table 1 and table 2 illustrates that the detecting parameters of the buried objects in the survey environment having noticeably appropriate error (lower than 10%).

The accuracy of the proposed method is confirmed through the data analysis on typically theoretical models. The next job is going to the application of this technique to analyze the actual GPR data which was measured by the team from Geophysics Department, Faculty of Physics and Engineering Physics, University of Science, VNU Ho Chi Minh City.

3.2. Actual data
3.2.1. Actual data 1 - The underground telecommunication tube

GPR data was recorded by Duo detector (IDS, Italia), using antenna at frequency of 700 MHz. Three parallel profiles LZZ10018, LZZ10019, LZZ10020 and 1.50m spacingwere done at 3/2 Street, NinhKieu District, Can Tho City on Friday , September 21, 2018 by our group. Each measurement lineon the ground went through anomaly object and the length of the profile was4.70 m, with the step size of $dx = 0.02784$ m. Fig. 3 shows the data of underground telecommunication tube in three dimensional performance.
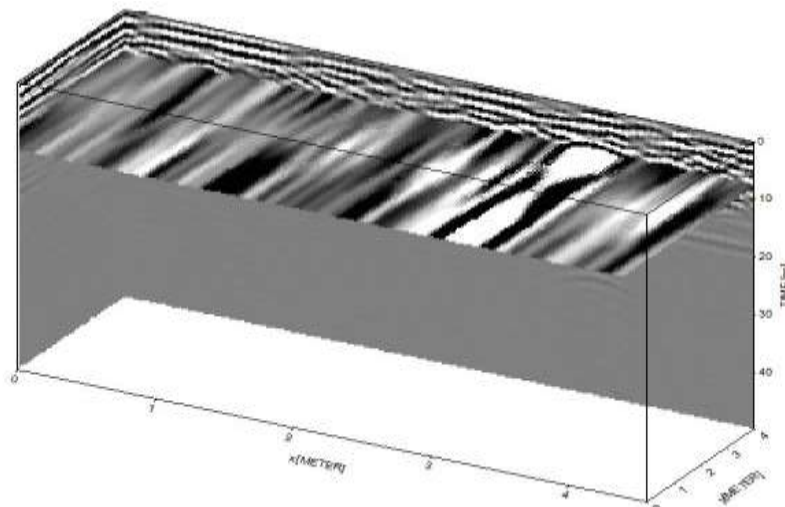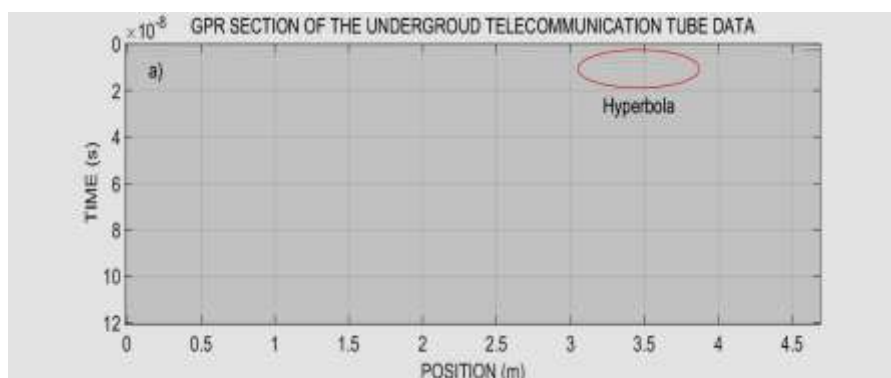

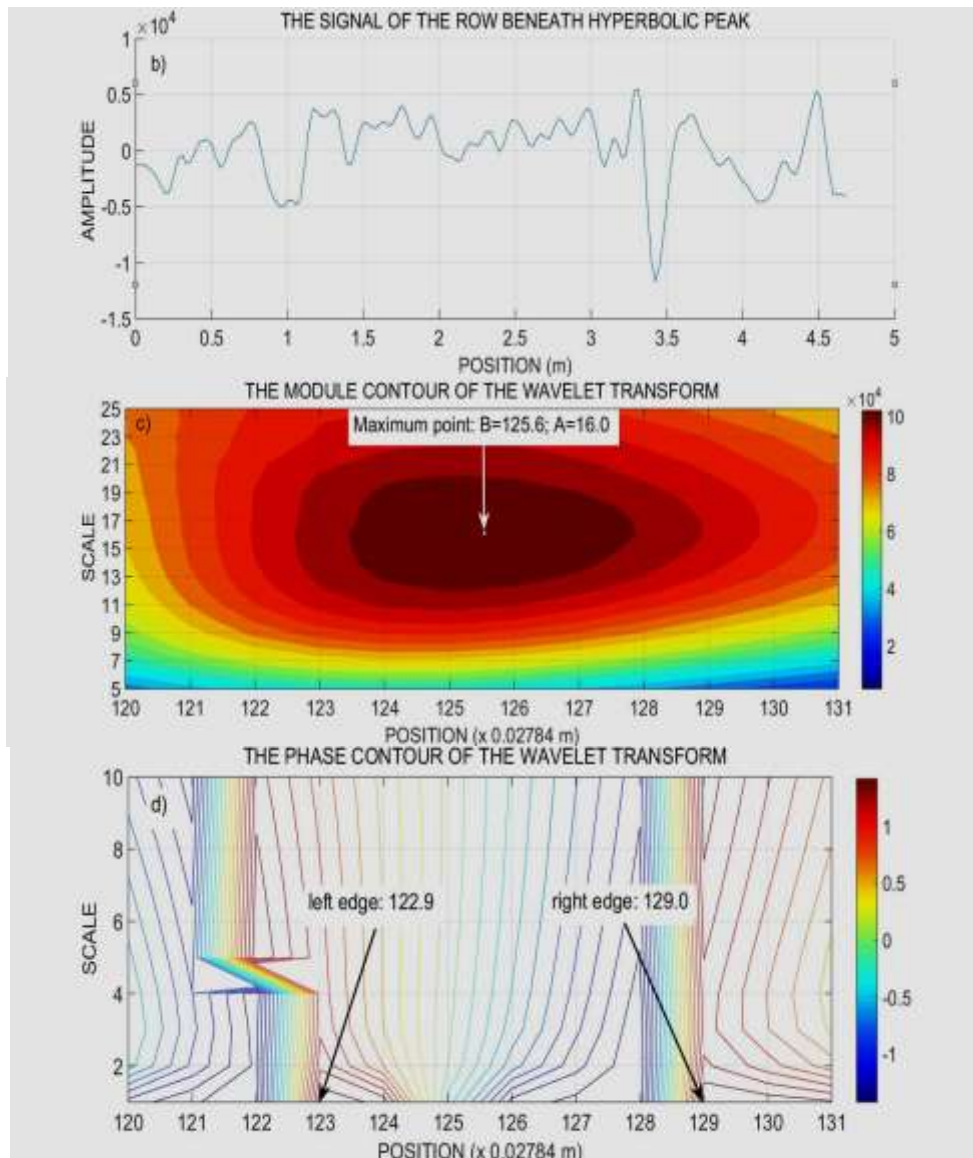**Fig. 3.**3D-GPR data of the underground telecommunication tube

To begin with, the profile LZZ10018 has been selected to process. Analyzed results have been indicated in the Fig. 4.

According to the information was provided by VNPT Can Tho, the size of buriedtelecommunication tube is 0.185 m and itissituated at horizontal coordination x = 3.40 m along the survey route and vertical coordination is z = 0.41 m.

As can be seen in the Fig. 4c, the maximum point of the wavelet transform coefficients locating at ($B =$ 125.6; $A = 16.0$), and based on the Fig. 4d, the left edge and the right edge coordination of the tubeare 122.9 and 129.0respectively.Thus, the position, depth and size of the pipeare estimated by the equation (10), (11) and (12). Thecalculativeresultsare representedin table 3.Taking a similar analysis for the other profiles and connecting the calculativeresults from three survey profiles, we obtained the summarized results in the Fig. 5.

Fig. 4. The graphs of the profile LZZ10018. a) GPR section of the underground telecommunication tube data,b) The signal of the row beneath hyperbolic peak, c) The module contour of the wavelet transform, d) The phase contour of the wavelet transform

**Table 3:** Interpretative results of the profile LZZ10018

| Position	x= 125.6 × 0.02784 = 3.497 m	Relative error	2.9%
Depth	z = 16.0 × 0.02784 = 0.445 m	Relative error	8.5%
Size	D = (129.0-122.9) × 0.02784 = 0.170 m	Relative error	8.1%
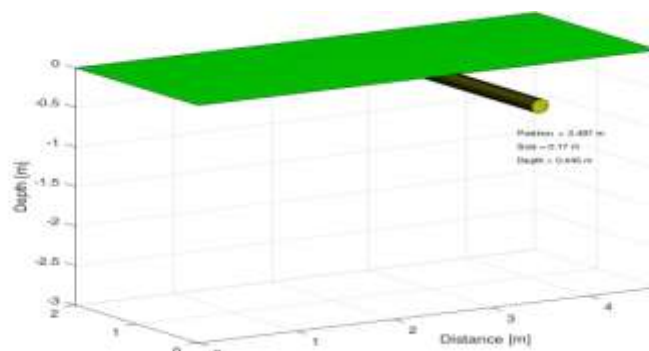
Fig. 5.3-D visualization of the actual data 1

3.2.2. The water electrical tubeand drainagepipewere close buried

GPR data was recorded by Duo detector (IDS, Italia), using antenna at frequency of 250 MHz. Three parallel routes LZZ20015, LZZ20016,LZZ20017 and 1.50m spacingwere done at B25Road, Hung Phu Zone, Cai Rang District, Can Tho City on Saturday , September 22, 2018 by our group.Each measurement profile on the ground went through anomaly objects and the length of the profile was 8.0m, with the step size of $dx = 0.02784$ m.The data of water drainage pipe and electrical tube in three dimensional display isrepresented in the Fig. 6.
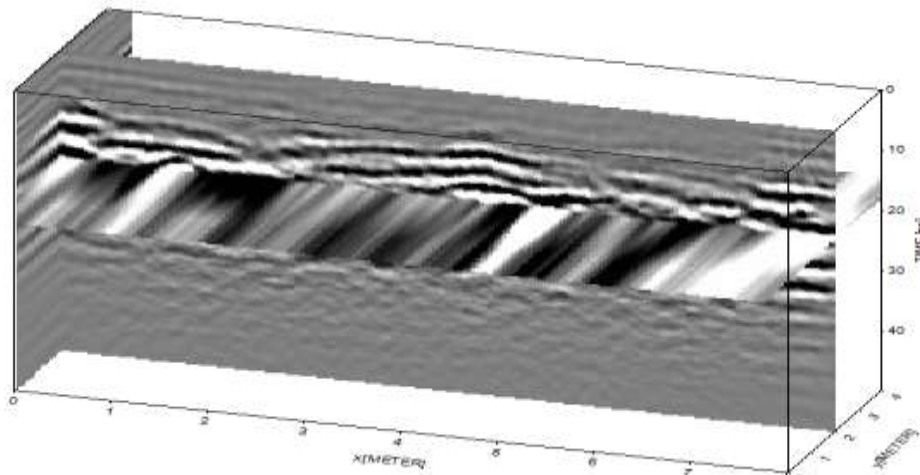
Fig. 6.*3D-GPR data of the water drainage pipe and electrical tube*
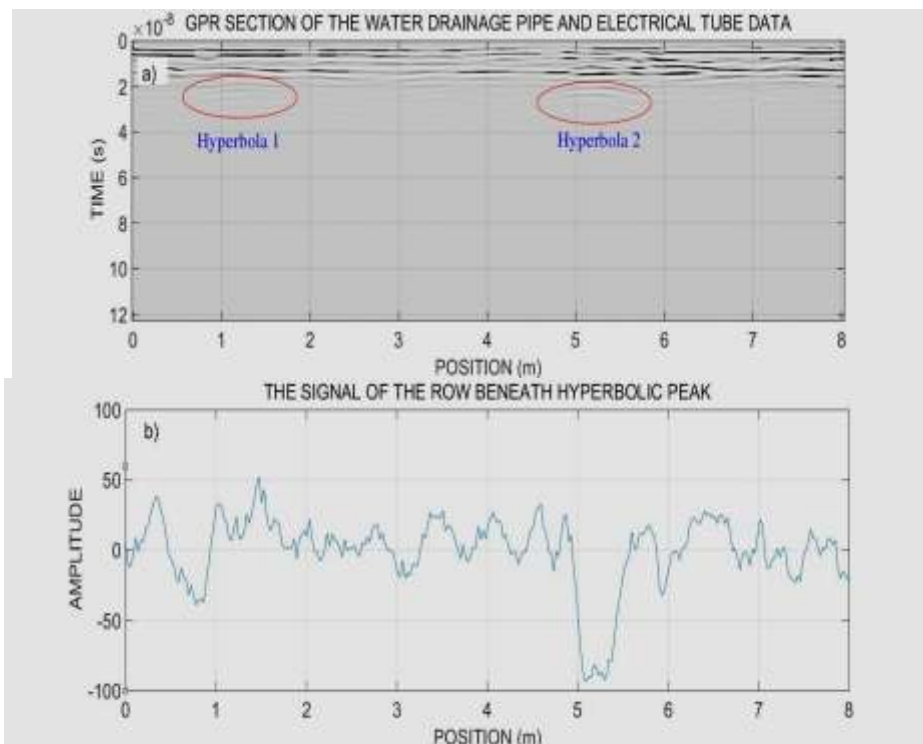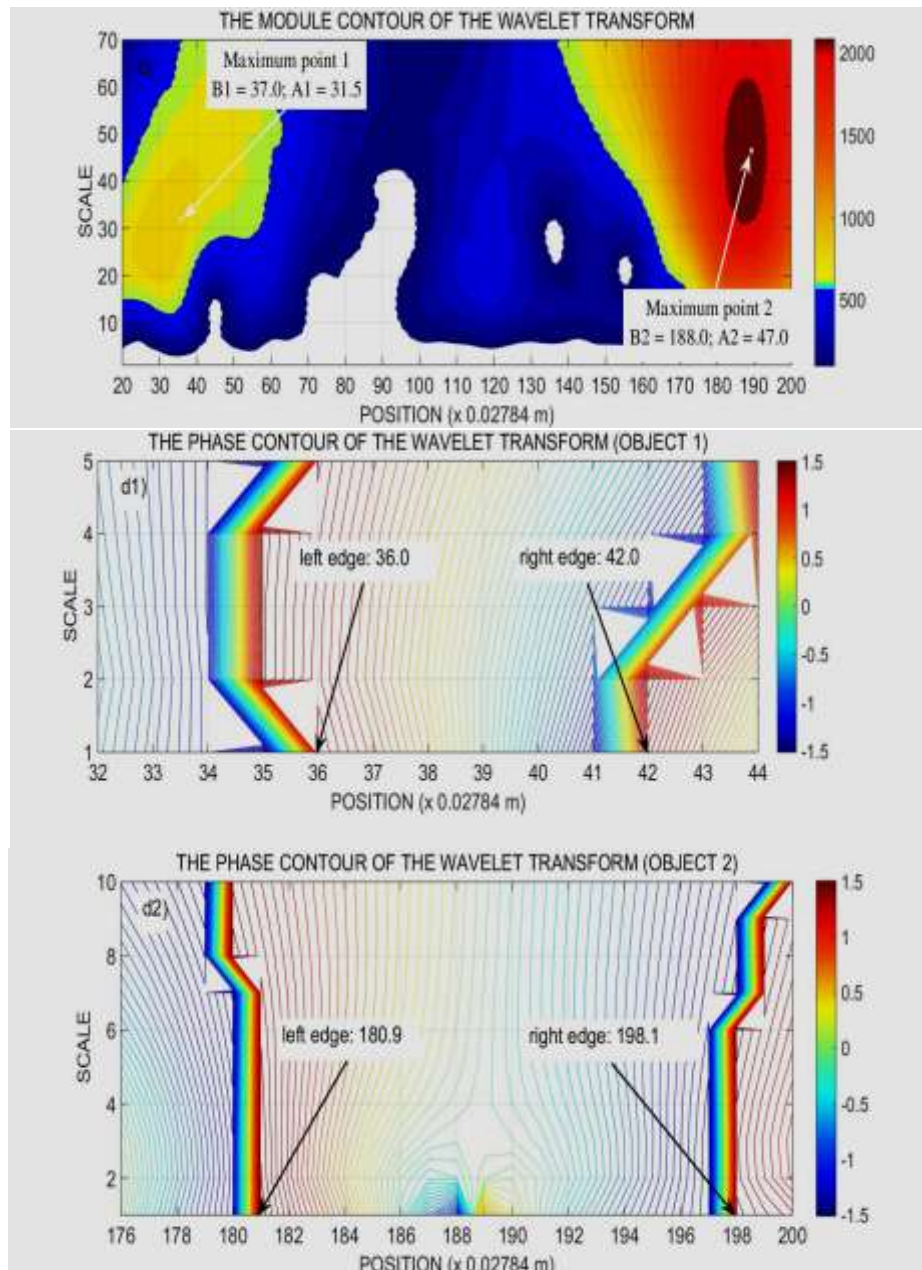
Fig. 7. The graphs of the profile LZZ20015. a) GPR section of the water drainage pipeand electrical tube data, b) The signal of the row beneath hyperbolic peak, c) The module contour of the wavelet transform, d1 and d2) The phase contour of the wavelet transform for object 1 and object 2 respectively.

Firstly, we select the profile LZZ20015 for processing. Analyzed results have been presented in the Fig. 7.

According to the information was provided by Can Tho Housing Development Joint Stock Company, the size of electrical tube and drainage pipeare 0.16 m and 0.53 m in turn, and they are located at horizontal coordination $x_1 = 1.00$ m and $x_2 = 5.30$ m along the survey route and vertical coordination are $z_1 = 0.95$ m and $z_2 = 1.45$ m.

As can be seen in the Fig. 7c, the maximum points of the wavelet transform coefficients locating at ($B_1 = 37.0$; $A_1 = 31.5$) and ($B_2 = 188.0$; $A_2 = 47.0$), and based on the Fig. 7d1 and 7d2, the left edge and the right edge coordination of the anomaly object 1 and object 1 are (36.0; 42.0) and (180.9; 198.1)in turn.Thus, the position, depth and size of the pipes are estimated by the equation (10), (11) and (12). Thecalculativeresultsare representedin table 4.Taking a similar analysis for the other profiles and connecting the calculativeresults from three survey profiles, we obtained the summarized results in the Fig. 8.

Table 4: Interpretative results of the profile LZZ20015

Position	$x_1 = 37.0 \times 0.02784 = 1.030$ m	Relative error	3.0%
	$x_2 = 188.0 \times 0.02784 = 5.234$ m	Relative error	1.2%
Depth	$z_1 = 31.5 \times 0.02784 = 0.877$ m	Relative error	7.7%
	$z_2 = 47.0 \times 0.02784 = 1.308$ m	Relative error	9.8%
Size	$D_1 = (42.0-36.0) \times 0.02784 = 0.167$ m	Relative error	4.2%
	$D_2 = (198.1-180.9) \times 0.02784 = 0.479$ m	Relative error	9.6%
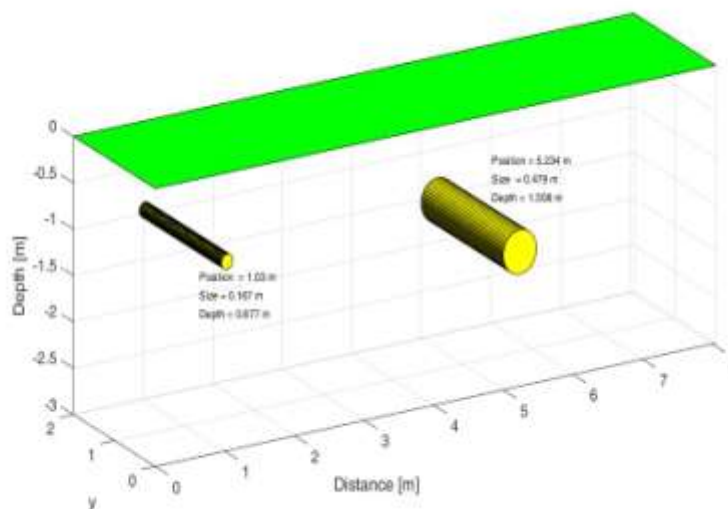
Fig. 8.3-Dvisualizationof the actual data 2

From table 1 to table 4, it is easy to compare the relative error for computed position with depth and size of the buried pipe using the CWT with Farshad-Sailhac wavelet function. Due to the GPR attenuation when penetrating to the environment, depth and size errors is usually larger than error of position.

The GPR data analysis bases on CWT taken a major role for determination of the depth, location and size of the adjacent objects buried shallow in a heterogeneous environment, this could not be done by a radar machine itself. Then, for the next step, we taken out anomalies from the environment or put another pipeline into the ground. It is going to rather easier, saving constructive time and improving the economic efficiency.

IV. CONCLUSION

The GPR data interpretative process using CWT with Farshad-Sailhac wavelet function for the determination of depth, position and the size of the buried objects has been established and applied successfully. We have tested the process to analyze two typically theoretical models and twoactual models. The theoretical models built in this paper are linked very closely to the objects studied in practice in order to verify the reliability of the proposal method before of the application on the real data. The final results for the theoretical models in determining the position, the depth and the size have relative error less than or equal to 2.6%, 8.0% and 8.0% in turn. For the actual models, the relative error in detecting the position, the depth and the size are less than or equal to 3.0%, 9.8% and 9.6% respectively.These relevant results indicated that using CWT and WTMM technique provides an orientation to explain the GPR data efficiently. If the researchers deeply combine the presentational technique and traditional methods for GPR interpretation, the identification of many bodies in designing and mapping urban underground construction workswill become more effective.

REFERENCES

[1]. Kumar, P., Foufoula-Georgiou, E., Wavelet analysis for geophysical applications, Reviews of Geophysics, 35, 4, 385-412 (1997).
[2]. Ouadfeul, S., Automatic lithofacies segmentation using the wavelet transform modulus maxima lines (WTMM) combined with the detrended fluctuation analysis (DFA), 17th International geophysical congress and exhibition of Turkey, Expanded abstract (2006).
[3]. Ouadfeul, S., Very fines layers delimitation using the wavelet transform modulus maxima lines WTMM combined with the DWT, SEG SRW, Expanded abstract, (2007).
[4]. Ouadfeul, S, Aliouane, L., Eladj, S., Multiscale analysis of geomagnetic data using the continuous wavelet transform, Application to Hoggar (Algeria), SEG Expanded, Abstracts 29, 1222; doi:10.1190/1.3513065 (2010).
[5]. Fedi, M., Quarta, T, Wavelet analysis for the regional – residual separation of potential field anomalies, Geophysical Prospecting, Vol.46, pp. 507-525 (1998).
[6]. Dau, D. H., 2013. Interpretation of geomagnetic and gravity data using continuous wavelet transform. Vietnam National University Ho Chi Minh City Press. 127 pp.

[7].   Sheng H. N., Yan H. H., Kuo F. L., Da C. L., Buried pipe detection by ground penetrating radar using the discrete wavelet transform, Elsevier, Computers and Geotechnics. 37, 2010, pp. 440-448.

[8].   Fiorentine A., and Mazzantini L., Neuron inhibition in the human fovea: A study of interaction between two line stimuli, Attidella Fondazione Giorgio Ronchi, 21, 1966, pp. 738-747.

[9].   Mallat S., Hwang W. L., Singularity Detection and Processing with Wavelets, IEEE Transactions on information Theory, 38 (2), 1992, pp. 617-643.

[10].   Cook J. C., Proposed monocycle-pulse VHF radar for airborne ice and snow measurements. Journal of the American Institute of Electrical Engineers, Transactions on Communication and Electronics, 1960, 79: 588-594.

[11].   Moffatt D. L., Puskar R. J., A subsurface electromagnetic pulse radar, Geophysics, 41, 1976, pp. 506-518.

[12].   Benson A. K., Applications of ground penetrating radar in assessing some geological hazards–examples of groundwater contamination, faults, cavities. Applied Geophys. 1995, 33: 177-193.

[13].   Tin, D. Q. C., Dau, D. H., 2016, Interpretation of the geomagnetic anomaly sources in the Mekong Delta using the wavelet transform modulus maxima., Work. on Capacity Build. on Geo. Tech. in Mineral Exp. and Assess. on Land, Sea and Island, Ha Noi, pp. 121-128.

[14].   Van, N. T., Giang, N. V., 2013. Ground penetrating radar – Methods and Applications.Vietnam National University Ho Chi Minh City Press. 222 pp.